inorganics

MDPI

Article

Characterization, Catalytic and Microbial Activities of Sustainable $CoFe_2O_4$ Nanoparticles via *Adansonia digitata* L. (Baobab) Fruit Pulp Extract Assisted by Microwave Hydrothermal Method

Amel Taha * and Norah Alsadun *

Department of Chemistry, College of Science, King Faisal University, P.O. Box 400, Alahsa 31982, Saudi Arabia
* Correspondence: ataha@kfu.edu.sa (A.T.); nalsadoun@kfu.edu.sa (N.A.)

Abstract

Novel biogenic cobalt ferrite nanoparticles were prepared biologically using *Adansonia digitata* L. (Baobab) Fruit Pulp Extract, assisted by a microwave heating method. The utilization of *Adansonia digitata* L. (Baobab) Fruit Pulp Extract assisted by microwave heating is considered an eco-friendly method that is environmentally sustainable and inexpensive in terms of energy consumption and large-scale production. Different techniques were used to characterize plant extract-mediated nanoparticles, including X-ray diffraction (XRD), Fourier transform infrared spectroscopy (FTIR), scanning electron microscopy (SEM), transmission electron microscopy (TEM), and N_2 adsorption–desorption analysis. The XRD analysis revealed single-phase crystalline structures with a mean size of 31.5 nm. In SEM and TEM studies, the nanoparticles took different morphologies, such as regular and spherical shapes. The bio-synthesized nanoparticles showed high removal efficiency as adsorbent components in MO removal, for example, of organic dye. The influences of different factors on the adsorption process, such as MO concentration, solution pH, and doses used, were tested based on the amount of adsorbent used. The kinetic and isotherm study results revealed that pseudo-second-order kinetics models and the Freundlich sorption isotherm model fit the adsorption process of MO on nano adsorbents well. Additionally, the antimicrobial assessment of $CoFe_2O_4$ NPs was tested against five species of human pathogenic bacteria, as well as one fungal species. The results show that $CoFe_2O_4$ NPs exhibit higher inhibition activity against the examined microorganisms.

Keywords: *Adansonia digitata* L. (Baobab) Fruit Pulp; $CoFe_2O_4$ NPs; catalytic activity; antimicrobial

Check for updates

Academic Editor: Gang Hong

Received: 16 May 2026
Revised: 10 July 2026
Accepted: 12 July 2026
Published: 2 August 2026

1. Introduction

The rapid development of the textile, printing, and pharmaceutical industries has led to the discharge of large quantities of synthetic dyes and pathogenic microorganisms into water bodies, posing a significant threat to environmental sustainability and human health. Among various pollutants, anionic azo dyes, such as methyl orange (MO), are particularly notorious for their stability and toxicity [1,2], while the rise of antibiotic-resistant bacteria has intensified the search for more effective antimicrobial agents [3,4]. In this context, nanotechnology has emerged as a transformative field, offering high-performance materials like spinel ferrite nanoparticles for diverse environmental and biomedical applications [5]. Spinel ferrite materials are metal oxides that have spinel structures and take a general chemical formula AB_2O_4, where A and B refer to different divalent metal cations, which are placed at tetrahedral and octahedral sites, respectively. The appearance of different metal cations in the spinel structure with different ratios has a significant impact on the ferrite's physicochemical properties. Spinel ferrite displayed unique and notable properties, such as crystalline and magnetic properties, so it attracted great attention in different fields, such as physics, chemistry, materials science, and engineering [6]. Ferrite with magnetic properties, such as $CoFe_2O_4$ [7,8], $MnFe_2O_4$ [9], $ZnFe_2O_4$ [10], and $NiFe_2O_4$ [11] nanoparticles, are recognized as promising materials, since they show high chemical and thermal stability, as well as unique structural, magnetic, optical, and electrical properties, so they are widely used in different applications, including photocatalysis, sensors, catalysis, and medical applications. During the last few years, spinel ferrites have been widely used as an effective adsorbent for dye degradation. In addition to their advantages as nanostructured adsorbents, ferrites also offer easy recovery of the adsorbent from treated solution due to their magnetic properties [12,13]. Among these, nanoferriate cobalt ferrite ($CoFe_2O_4$) has attracted significant attention due to its strong magnetic anisotropy, moderate saturation magnetization, and excellent catalytic performance. These properties make $CoFe_2O_4$ an ideal candidate for magnetic separation in water treatment, where it can easily be recovered and reused after capturing pollutants [14–16].

Traditional chemical and physical synthesis approaches for $CoFe_2O_4$, such as sol–gel, hydrothermal, and coprecipitation, often involve toxic reducing agents, high energy consumption, and complex procedures, yielding hazardous by-products. Consequently, there has been a paradigm shift towards green synthesis, a sustainable and eco-friendly approach that utilizes biological entities, particularly plant extracts, as bio-reductants and capping agents. Plant-mediated synthesis is cost-effective, easily scalable, and avoids the use of toxic chemicals, making the resulting nanoparticles safer for environmental and clinical use [17–19]. The Adansonia genus belongs to the Malvaceae family, which has spread extensively across many African countries. It is commonly used by local populations due to its useful properties in food or for traditional medicine. Several studies have reported uses of A. digitata for medicinal purposes due to the presence of many compounds with biological activity. Baobab fruit pulp is known to be a rich source of minerals such as calcium and potassium and vitamins (vitamins C and A), and includes flavonoids, triterpenoids, steroids, phenolic acids, and proanthocyanins. These active compounds make Baobab fruit pulp show some biological activities such as analgesic, antipyretic, antibacterial, antiviral, antioxidant, and anti-inflammatory properties [20]. These compounds serve a dual role: they act as reducing and capping agents that help to stabilize nanoparticles and prevent agglomeration, thereby enhancing their functional surface properties. Using plant extracts in the synthesis of metal nanoparticles is considered an eco-friendly process compared to using conventional chemical methods. Through this route, hazardous chemicals are reduced as the green reducing and stabilizing agents available in the plant extracts are employed instead. Previous studies have successfully employed Baobab extracts to synthesize various metallic nanoparticles, demonstrating their effectiveness in producing stable, bioactive nanomaterials [21–23].

Numerous significant studies in the literature have discussed the plant-mediated synthesis of $CoFe_2O_4$. K. Kombaiah et al. prepared $CoFe_2O_4$ nanoparticles with interesting magnetic and optical properties via Okra plant extract [24]. Hibiscus rosa-sinensis flower and leaf extracts were used to prepare spherical nanoparticles with a very low energy bandgap and super-paramagnetic properties, which were used as an effective catalyst in photo-catalytic degradation of methylene blue and as an anti-microbial agent [25]. Sesame (*Sesamum indicum* L.), rosemary (*Salvia rosmarinus*), and citrus limon were also used to prepare $CoFe_2O_4$ nanoparticles using other methods such as sol–gel, self-combustion, wet ferritization, and the combustion method, and have been applied in various applications [26,27].

Despite the potential of $CoFe_2O_4$ nanoparticles in many fields, no research has reported the use of fruit pulp from *Adansonia digitata* extract as a capping agent; additionally, there is no current data on the combination of fruit pulp from *Adansonia digitata* extract with the microwave-assisted hydrothermal method in the synthesis of $CoFe_2O_4$ nanoparticles.

The application of green-synthesized $CoFe_2O_4$ for the removal of MO has shown high efficiency, typically following the Langmuir monolayer adsorption model and pseudo-second-order kinetics. Under UV or visible light irradiation, these nanoparticles also act as photocatalysts, generating reactive oxygen species (ROS) that oxidatively degrade dye molecules into harmless CO_2 and H_2O [28,29]. Furthermore, $CoFe_2O_4$ nanoparticles show important antimicrobial activity against both Gram-positive (e.g., *Staphylococcus aureus*) and Gram-negative (e.g., *Escherichia coli*) pathogens. This bactericidal effect is attributed to the generation of ROS and direct physical interactions with microbial cell membranes, leading to cell disruption and death [30]. This study aims to synthesize spinel $CoFe_2O_4$ nanoparticles using an extract from the fruit pulp of *Adansonia digitata* and investigate their multifaceted performance in the remediation of Methyl Orange-contaminated water and their inhibitory effects against common bacterial strains. By integrating green chemistry with magnetic nanotechnology, this research contributes to the development of sustainable and reusable solutions for environmental protection and public health [31].

2. Results and Discussion

2.1. Material Characterization

The crystallographic data obtained by X-ray diffraction analysis of biosynthesized $CoFe_2O_4$ nanoparticles are presented in Figure 1a. The sample exhibits diffraction peaks at (200), (311), (400), and (511) at $2\theta = 28.06°$, $33.02°$, $47.2°$, and $58.6°$ that are parallel to the cubic spinel ferrite structure according to standard ICDD diffractogram card number JCPDS NO. 22-1086 [19,22]. The crystallite size of the sustainably synthesized $CoFe_2O_4$ cubic spinel ferrite nanoparticles was calculated by the Debye–Scherrer formula [10], and the average of their calculated size was 24 nm. Due to their atomic radius (200 pm), the spinel ferrites were designed to contain cobalt material. Iron-coupled cobalt materials have tetrahedral sites. The mixture of iron and cobalt metals increased the oxygen vacancy for better formation of the nanostructure [32].

FT-IR spectra of the prepared $CoFe_2O_4$ nanoparticles with BFPE were studied for functional groups that may be involved in the synthesis of the prepared nanomaterial. As shown in Figure 1, the FTIR analysis of aqueous BFPE exhibited a wide band at 3373 cm^{-1}, which was attributed to the stretching vibrations of –OH and the stretching of aromatic and aliphatic compounds. The spotted peaks at 2916 cm^{-1} were assigned to C-H stretching and CH_2 group vibrations. In addition, the presence of a strong, sharp band around 1655 cm^{-1} was assigned to the C=O stretching vibration of aromatic structures [21].

The IR spectrum of the $CoFe_2O_4$ nanoparticles, presented in Figure 1b, displays small peaks in the range of 3160–3500 cm^{-1}, which could be attributed to the H-bonded and –OH groups of internal water molecules. The appearance of bands at 618 and 420 cm^{-1} is attributed to stretching in the M-O bond of ferrite in the octahedral and tetrahedral groups, respectively, which supports the occurrence of spinel cobalt ferrite [33,34]. This finding confirms the successful synthesis of $CoFe_2O_4$ nanoparticles.

Vibrating Sample Magnetometry (VSM) analysis was used to study the magnetic properties of the sustainably synthesized $CoFe_2O_4$ nanoparticles, and the results are shown in Figure 2. The as-prepared nanoparticles display a typical magnetic hysteresis loop and exhibit ferromagnetic behavior with a value of saturation magnetization (MS) of about 56 emu/g and a remanence (Mr) of 25.30. These results are consistent with those reported by Duo et al. and Ali Modabberas et al., with Ms and Mr values of 47.1 emu/g and 27.5 emu/g, respectively, at room temperature [35]. The distribution of positive ions in tetrahedral and octahedral locations affects the magnetic properties of spinel nanoparticles, which play an important role in determining the magnetic properties of spinel material [36,37].

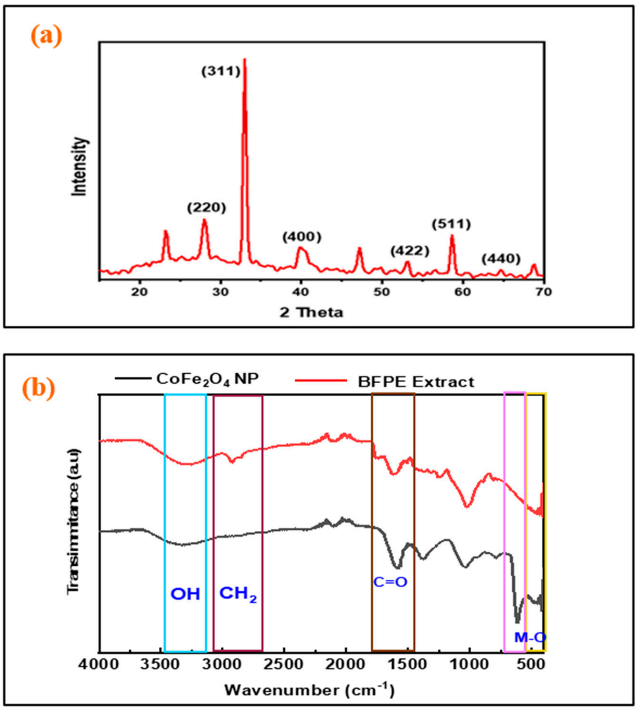

Figure 1. (**a**) XRD spectrum of $CoFe_2O_4$ nanoparticles, (**b**) FTIR spectra of $CoFe_2O_4$ nanoparticles and Baobao fruit bulb extract.

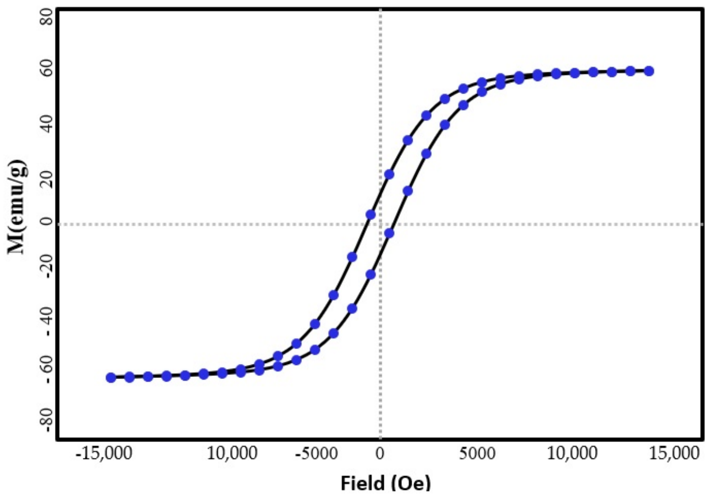

Figure 2. VSM spectrum of biosynthesized $CoFe_2O_4$ nanoparticles.

The N_2 adsorption/desorption of $CoFe_2O_4$ nanoparticles, analyzed by the BET method, is shown in Figure 3a,b. According to the IUPAC classification, $CoFe_2O_4$ nanoparticles had an IV isotherm type, which is characteristic of a mesoporous structure [34]. The BET-specific surface area calculation, pore volume, and pore size of $CoFe_2O_4$ nanoparticles were found to be 51 m^2g^{-1}, 0.097 cm^3g^{-1}, and 1.77 nm, respectively.

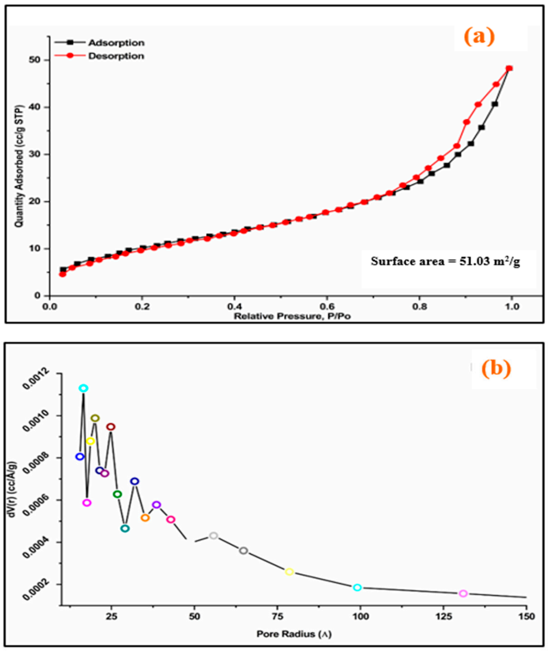

Figure 3. (**a**,**b**) N_2 adsorption/desorption isotherm curves of $CoFe_2O_4$ nanoparticles obtained from nitrogen gas.

The morphology of the biosynthesized $CoFe_2O_4$ nanoparticles was studied using SEM techniques. Figure 4a–c represents SEM images of $CoFe_2O_4$ nanoparticles at different magnifications. The biosynthesized $CoFe_2O_4$ nanoparticles displayed a spherical form and were uniformly dispersed across the surfaces of the particles. The phytochemical constituents present in Baobao fruit bulb extract, such as terpenoids and flavanones, serve as capping agents for the growth of metal oxides [26,38,39]. Figure 4d displays the EDX analysis of the $CoFe_2O_4$ nanoparticles. The presence of Fe, Co, and O elements confirmed the purity of the synthesized nanoparticles. The quantitative Co: Fe ratio from the EDX spectrum is represented in Table 1.

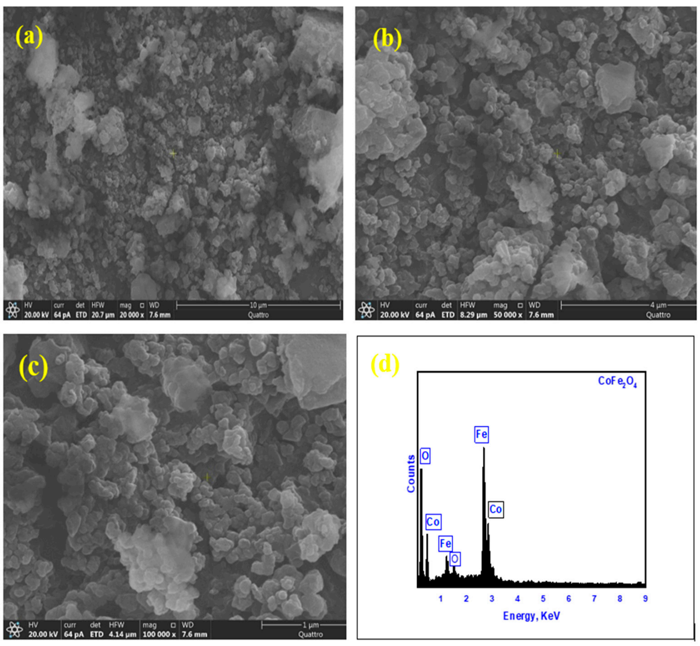

Figure 4. SEM images (**a**–**c**), (**d**) EDX spectrum of $CoFe_2O_4$ nanoparticles.

Table 1. Quantitative analysis from EDX spectrum of $CoFe_2O_4$ nanoparticles.

EL	AN	Series	[wt%]	[at. %]
O	8	K-series	31.53	62.03
Fe	26	K-series	49.09	25.09
Co	27	K-series	19.38	12.88
Total			100.00	100.00

Figure 5a,b show HR-TEM images of $CoFe_2O_4$ nanoparticles. From the images, it is clear that $CoFe_2O_4$ nanoparticles occur in almost spherical and regular shapes. The particle size histogram was calculated using ImageJ software version 1.54 K, as shown in Figure 5c. The calculated average nanoparticle size from the TEM measurement was 31.5 nm [39]. These findings prove the effective production of $CoFe_2O_4$ nanoparticles using Baobab fruit bulb extract as a capping agent. Figure 5d represents the selected area electron diffraction pattern (SAED) of the $CoFe_2O_4$ nanoparticles, which reveals multi-layered patterns, signifying the polycrystalline nature of the produced $CoFe_2O_4$ nanoparticles [40].

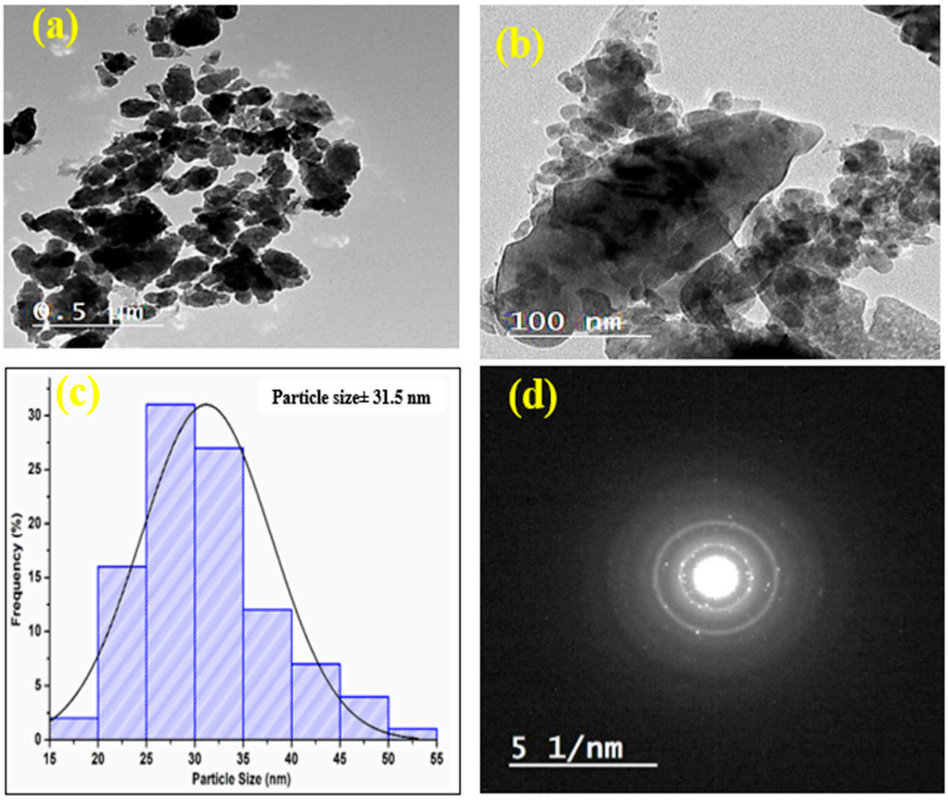

Figure 5. TEM images (**a**,**b**) at different magnifications. The histogram of the particle size distribution (**c**,**d**) the selected area electron diffraction pattern (SAED) of the $CoFe_2O_4$ nanoparticles.

2.2. Adsorption Analysis

2.2.1. Zero-Point Charge (ZPC)

Zero-point charge is considered a crucial parameter that shows the ionization performance of an adsorbent. The adsorbent is negatively charged at pH > ZPC, at pH = ZPC, and positively charged at pH < ZPC. Figure 6a displays the plot of pHi vs. ΔpH; the zero charge was determined to be 3.7, as shown in the figure.

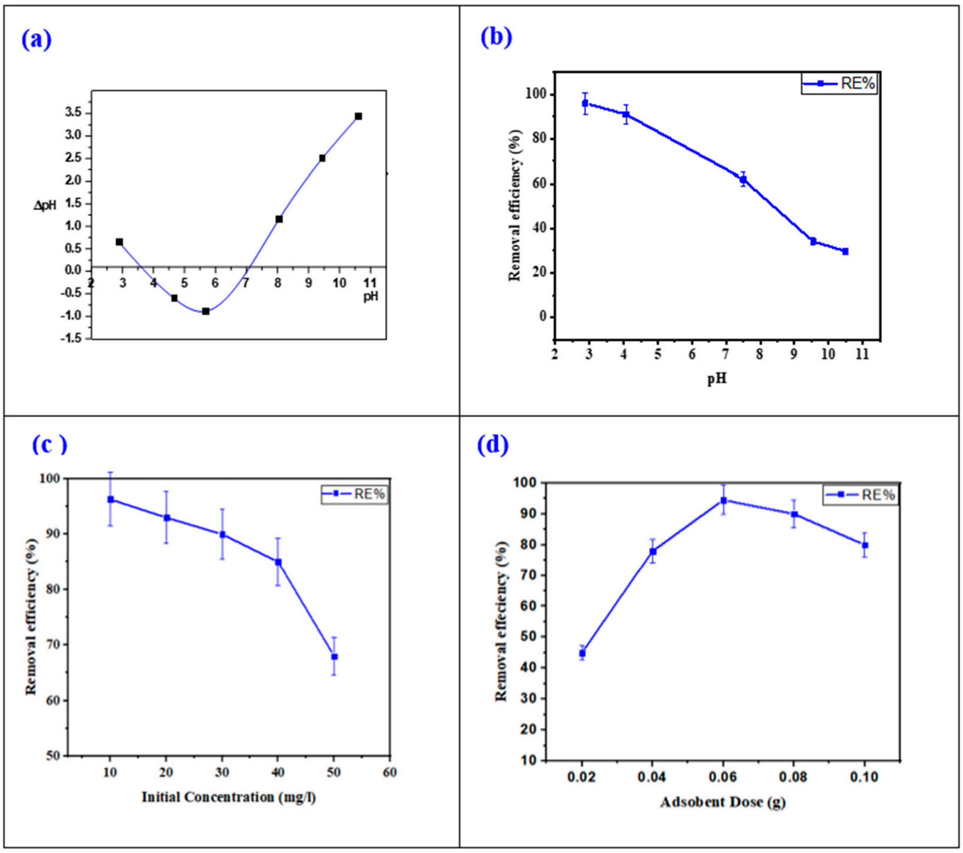

Figure 6. (**a**) Zero-point charge measurements as a function of pH for $CoFe_2O_4$ nanoparticles. (**b**) Effect of pH of solution on the MO removal efficiency from aqueous solution. Conditions: (MO concentration: 10 mg/L, 0.06 g adsorbent dose, and 24 h contact time. (**c**) Effect of initial MO concentration on the removal efficiency. Conditions: (pH = 2.8; 0.06 g adsorbent dose and 24 h contact time). (**d**) Effect of initial MO concentration on the removal efficiency. Conditions: (pH = 2.8; 0.06 g adsorbent dose and 24 h contact time).

2.2.2. Effect of pH

Solution pH plays an important role in the efficiency of MO removal since it has a significant effect on the nano-adsorbent active sites as well as the degree of ionization of MO [41]. To examine the influence of pH on MO sorption by $CoFe_2O_4$ nanoparticles, the pH values were varied from 2.0 to 11.0 while the initial MO concentration (10 mg, contact time 24 h, and $CoFe_2O_4$ dose 0.05 g) was fixed. With an increase in solution pH from 2 to 11, the removal percentage efficiency of $CoFe_2O_4$ nanoparticles decreases. This can be explained by the fact that the $CoFe_2O_4$ nanoparticles' surface is expected to have a positive charge at lower pH values, which could result in it being strongly attracted to the dye's negative groups (sulfonate) [7]. As is clear from Figure 6b, the maximum percentage of MO removal (97.5%) was achieved at a pH of around 2.8. The adsorption percentage (R%) started to decrease when increasing pH from 2.5 to 10.0; only 29% removal efficiency was achieved at pH 11.0. This is mainly owing to the deprotonation of the $CoFe_2O_4$ nanoparticles' surface, since the zero-charge point was determined to be 3.7, so beyond this point it becomes less positive and passes into a negative form. Therefore, the repulsion forces increase and restrict the approach of MO to the sorbent surface [24,42].

2.2.3. Effect of Initial Dye Concentration

To examine the effect of MO initial concentration, a varied concentration range (10–50 ppm) was used while keeping other parameters fixed. It is clear from Figure 6c that with the increasing MO concentration, the percentage of removal efficiency gradually decreased. The highest percentage of MO removal (96.8%) was obtained at a 10 ppm concentration. When the concentration of MO increased, the removal efficiency decreased [43]. The high percentage of efficiency of MO removal using $CoFe_2O_4$ nanoparticles at a low initial concentration might be associated with the availability of active sites on the surface area. When the concentration increased from 10 to 50 ppm, the percentage of removal efficiency decreased to 61.2%. This could be explained by the limitation of empty active sites when using a constant amount of $CoFe_2O_4$ nanoparticles, and the concentration being increased, which raises the saturation of surface-active sites [44].

2.2.4. Effect of Adsorbent Dose

One of the most significant and effective factors affecting dye removal efficiency is the adsorbent amount, since it controls the adsorbent capacity for a given specific amount of the adsorbate. To study the effect of adsorbent dosage on MO removal efficiency, numerous dosages (0.02–0.10 g) of $CoFe_2O_4$ nanoparticles were tested. This effect was examined using 20 mL of MO solution under fixed conditions (10 ppm, pH = 2.8, and T = 25 °C). As shown in Figure 6d, the MO removal efficiency (%) increased gradually from 45% to 94.5% when increasing the adsorbent dosage from 0.02 to 0.06 g. This is due to the availability of more active sites for dye adsorption. However, an increase in the $CoFe_2O_4$ nanoparticle dose results in a decrease in removal efficiency (80%). In fact, in aqueous solution, the dispersion of $CoFe_2O_4$ nanoparticles with low dosages is better, as most active sites on the $CoFe_2O_4$ nanoparticles' surface are totally open, which can motivate the MO molecules to access the adsorbent active sites and saturate quickly, resulting in a high percentage of removal [45]. Conversely, with an increase in adsorbent dose, due to collisions between the adsorbent particles, particle aggregation occurs, which reduces the surface area, and as a result of this, the percentage of MO removal from aqueous solution decreases [46].

2.2.5. Kinetics Studies

Kinetics studies were performed using 20 mL of 10 mg/L methyl orange, with a 0.06 g adsorbent dose at optimum pH 2.8. To study the kinetic behavior of $CoFe_2O_4$ nanoparticles on the adsorption of MO, two kinetic models were applied: pseudo-first-order and pseudo-second-order. The selection of the best-fit model will depend on the linear regression correlation coefficient values (R^2). The Lagergren rate Equation (1) represents the pseudo-first-order kinetic model.

$$ln(q_e - q_t) = lnq_e - k_1 t \tag{1}$$

where q_e and q_t (mg/g) are the amount of MO adsorbed at equilibrium and at time t, respectively, k_1 is the rate constant of the pseudo-first-order kinetic model (min^{-1}), and t is the time (min).

For the pseudo-second-order kinetic model, a linear form was represented using the following Equation (2).

$$\frac{t}{q_t} = \frac{1}{k_2 q_e^2} + \frac{1}{q_e} t \tag{2}$$

where k_2 (g/mg.min) is the rate constant of the second-order kinetic model.

The results of using different kinetic parameters for MO removal using $CoFe_2O_4$ nanoparticles are summarized in Table 2. Figure 7a,b show the results of the two models, and it is clear that pseudo-second-order achieved a higher correlation coefficient, R^2 (0.983), compared to pseudo-first-order (0.788). Furthermore, the experimental results (q_e, exp 10.71 mg/g) appear very close to the calculated values for the pseudo-second order (q_e, cal 9.89 mg). The results suggest that the results of the kinetic studies of MO onto $CoFe_2O_4$

nanoparticles are well-fitted to the pseudo-second order. Similar observations have been reported in the literature [4,10].

Table 2. Kinetic parameters for the adsorption of MO onto $CoFe_2O_4$ nanoparticles.

	Pseudo-First-Order	Pseudo-Second-Order
R^2	0.8084	0.9844
k (min^{-1})	0.011	0.0025

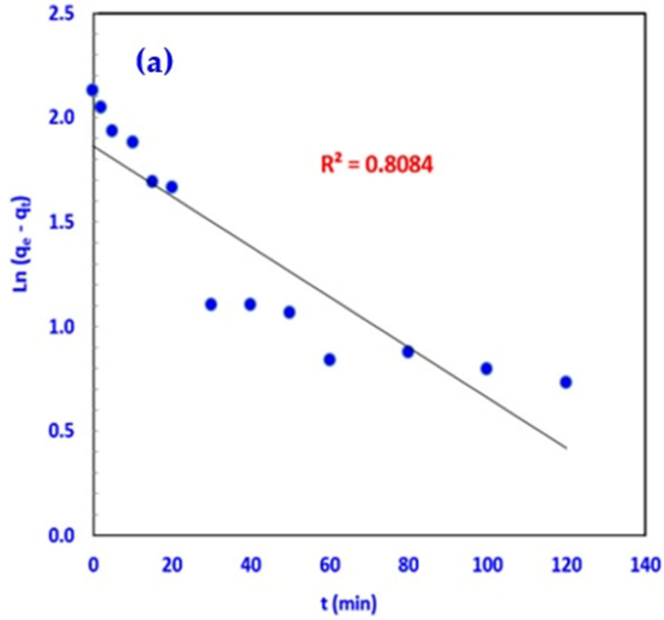

Figure 7. (**a**) Pseudo-first-order model, and (**b**) pseudo-second-order model for adsorption of MO onto $CoFe_2O_4$ nanoparticles.

2.2.6. Sorption Isotherm

To understand the interaction between adsorbent molecules and the sorbent needed to reach equilibrium, adsorption isotherm models are usually applied. Therefore, both the Langmuir and the Freundlich isotherms were applied to study the experimental adsorption equilibrium performance of $CoFe_2O_4$ nanoparticles during the adsorption of MO dye (Table 3). Langmuir and Freundlich adsorption isotherms are represented by Equations (3) and (4), respectively.

$$q_e = \frac{q_m\, K_L\, C_e}{I} + K_L\, C_e \quad (3)$$

$$q_e = K_F C_e{}^{\frac{1}{n}} \quad (4)$$

Table 3. Freundlich and Langmuir data for MO removal by $CoFe_2O_4$ nanoparticle$_s$.

System	q_m	K_L	K_F	1/n	R^2	Sorption Model
			0.08741	0.673	0.98615	Freundlich model
$CoFe_2O_4$	4.18	0.11			0.93265	Langmuir model

There is only a fixed number of sorption sites where adjacent adsorbed molecules do not hinder the process of further sorption. Equation (3) represents the Langmuir model linear form, where (q_e, mg/g) represents the amount of sorption at equilibrium, C_e represents the aqueous-phase concentration of adsorbate at equilibrium (mg/L), q_m is the monolayer sorption capacity (mg/g), and b refers to the Langmuir constant, which is related to the free sorption energy. The Freundlich model assumes the heterogeneity of the adsorption surface, where interactions between adsorbed molecules can occur and the sorption can be multilayer. Equation (4) represents the linear relationship of the Freundlich sorption isotherm, where K_F is the sorption capacity and $(1/n)$ is the intensity of sorption. Table 3 and Figure 8 represent the Langmuir and the Freundlich sorption constant values with the corresponding correlation coefficients. The linear correlation coefficient (R^2 = 0.986) value confirms that the system is fitted to the heterogeneous Freundlich isotherm better than the Langmuir model. The degree of surface heterogeneity can be described according to the $1/n$ value. With a smaller $1/n$ value, the surface is more heterogeneous, and at a value nearer to or equal to one, the surface is more homogeneous with binding sites [47,48].

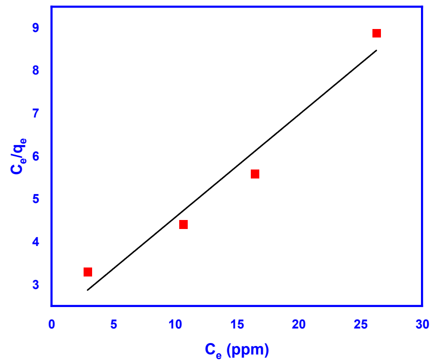

Figure 8. Freundlich fitting curves for MO adsorption onto $CoFe_2O_4$ nanoparticles.

2.2.7. Desorption and Mineralization Studies for $CoFe_2O_4$ Nanoparticles

It is very important to examine the possibility of regeneration and reuse of any adsorbent in multi-cycle systems for manufacturing applications. To test the reusability of $CoFe_2O_4$ nanoparticles, ethanol and acetone were selected in MO adsorption–desorption cycles, and because of their high dipole moments, both were selected [49]. To check the reusability of the adsorbent, six adsorption–desorption cycles in acetone and ethanol were conducted. The results are shown in Figure 9, and from the figure it is clear that after three cycles, the adsorption efficiency was still at the same level, and a minor decrease in the adsorption capacity was observed after six repeated cycles. It was observed that the removal efficiency for MO decreased by 8.35% using acetone and 18.00% using ethanol. These findings confirm the high-level recyclability of $CoFe_2O_4$ nanoparticles even after six adsorption–desorption cycles.

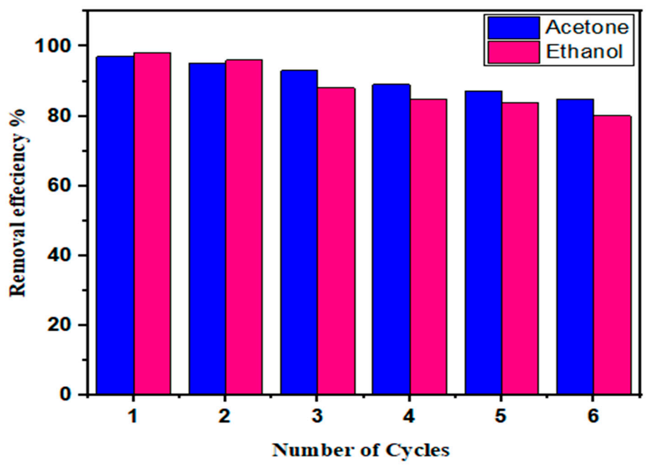

Figure 9. Reusability of $CoFe_2O_4$ nanoparticles.

https://doi.org/10.3390/inorganics14080204

For a better illustration of $CoFe_2O_4$ nanoparticles' catalytic performance, the mineralization study was investigated by the variation in total organic carbon (TOC), and the result was shown in Figure 10. Under the same optimal conditions for MO removal for 70 min. The mineralization rate for MO removal reached 80.1%. According to the results, the removal efficiency percentage of MO decreased in the recycle experiments. This may be attributed to the blocking of $CoFe_2O_4$ nanoparticles' pores by MO molecules after each use, which caused a decrease in adsorption and catalytic surface activity. Another reason was the slight leaching of metal ions on the catalyst [32]. The amounts of leaching of metal ions were measured as shown in Figure 10; the leaching efficiencies of Co and Fe ions were 0.45%, 1.3%, and 4.5%, respectively. Thus, the results confirmed the above decrease in the removal efficiency. All the results clarify that the $CoFe_2O_4$ nanoparticles had adequate physicochemical stability during the degradation process of MO.

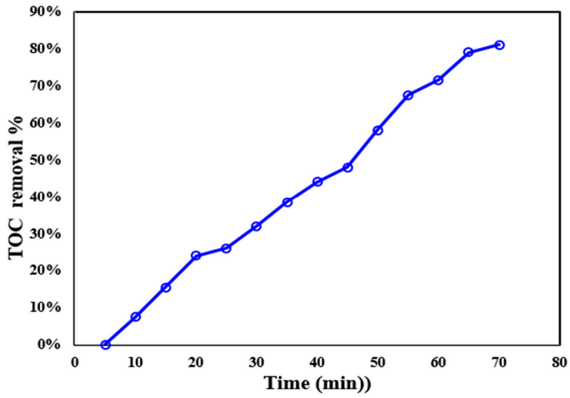

Figure 10. TOC removal over 70 min. Reaction conditions: (pH: 2.8; 0.06 g, adsorbent dose and 24 h, contact time).

2.2.8. Antibacterial Activity of $CoFe_2O_4$ Nanoparticles

Spinel ferrite materials, especially Cobalt ferrite ($CoFe_2O_4$), are well known for their high antimicrobial activity. An antibacterial assessment of $CoFe_2O_4$ NPs was conducted against five species of human pathogenic bacteria: *Escherichia coli*, Marsa, Pseudomonas aeruginosa, Klebsiella Pseudomonas, and Candida, as well as one fungal species. The antibacterial assessment of $CoFe_2O_4$ NPs is illustrated in Figure 11. As is clear from the figure, the sustainably synthesized particles showed an excellent range of inhibition towards the tested pathogenic microorganisms, including Gram-positive and Gram-negative bacteria and one fungal species. An increase in nanoparticle concentration and exposure time resulted in reduced absorbance across all test microorganisms. In other words, as $CoFe_2O_4$ NPs interact with the microorganisms, there is reduced OD600 due to inhibition of growth and cell proliferation. This is demonstrated by plotting the absorbance at 600 nm against the nanoparticle concentration or exposure [50]. From the graph, it is evident that E. coli displays the fastest absorbance decrease rate, implying its susceptibility. Candida sp. and Klebsiella pseudomonas, on the other hand, show comparatively higher absorbance values until intermediate levels of exposure and concentration before falling dramatically. This means that these two microorganisms are more resistant than *E. coli*. Notably, when the concentration or exposure increases further (40–60), the organisms display lower absorbance rates, hence verifying the high antimicrobial efficiency of $CoFe_2O_4$ NPs. The combination of plant extract and biosynthesized $CoFe_2O_4$ nanoparticles improved the bioactivity of the produced nanoparticles. The interaction between metal ions and the bacterial cells disturbed cell protection and accelerated the production of reactive oxygen species (ROS). The existence of Co and Fe ions as spinel ferrite improved the fragmentation of DNA, leading to interaction between metal ions and the cell membrane, which allowed the ferrite ions to enter the cell and upset its normal activities, leading to a deactivated state [51]. These changes in the cell system lead to the inactivation of cells and enhance their death.

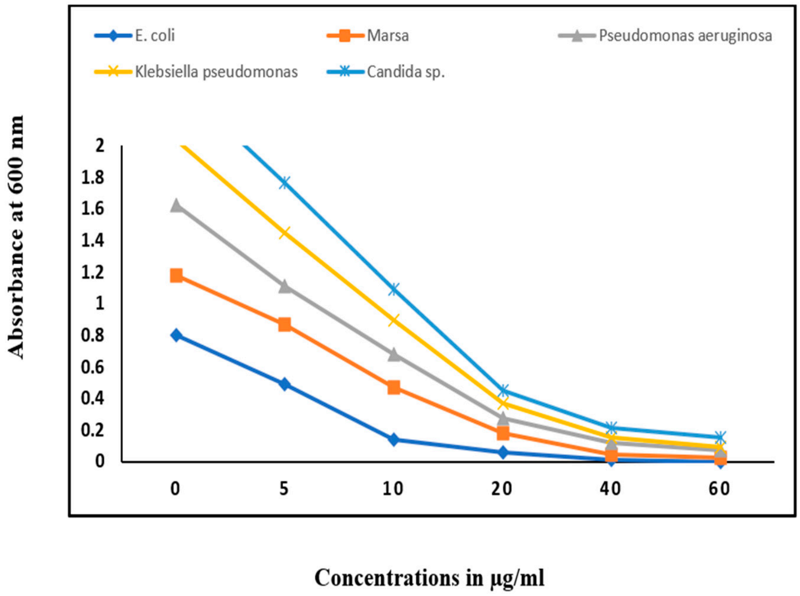

Figure 11. Antibacterial activity of $CoFe_2O_4$.

3. Materials and Methods

3.1. Materials

The starting materials of Cobalt (II) nitrate hexahydrate, Ferric nitrate nonahydrate, Whatman No. 1 filter paper, and Methyl orange (98% MO) were provided by Sigma-Aldrich. All materials used were of analytical reagent (AR) grade, without any modification during the synthesis time. *Adansonia digitata* L. (baobab) fresh fruit bulbs were obtained from the Alhasa local herbal market.

3.2. Baobab Fruit Pulp Extraction (BFPE)

To prepare the extract, 20 g of baobab fruit pulp was added to 200 mL of distilled water and boiled for 15 min. After that, the mixture was filtered using Whatman No. 1 filter paper to obtain a clear solution. The filtrate was then kept at 4 °C to undergo other tests. Starting materials of Cobalt (II) nitrate hexahydrate, Ferric nitrate nonahydrate, Whatman No. 1 filter paper, and Methyl orange (98% MO) were provided by Sigma-Aldrich Chemie GmbH, Steinheim, Germany.

3.3. Synthesis of Spinel $CoFe_2O_4$ Nanoparticles

Metal precursors Co $(NO_3)_2.6H_2O$ and $Fe(NO_3)_3$ in a molar ratio of 1:1 were dissolved in 100 mL of distilled water. This mixture was stirred for 10 min at room temperature. Next, 0.20 mL of stored BFPE was added to the metal mixture and stirred vigorously for 1 h. The mixture's pH was adjusted to 10 using 0.1 M KOH. The resulting solution was transferred to a microwave digestion system vessel at 200 °C and 50 atm for 30 min. The resultant materials were collected, washed three times with distilled water and ethanol 96%, and dried at 100 °C overnight. The synthesis protocol of $CoFe_2O_4$ nanoparticles is presented in Figure 12.

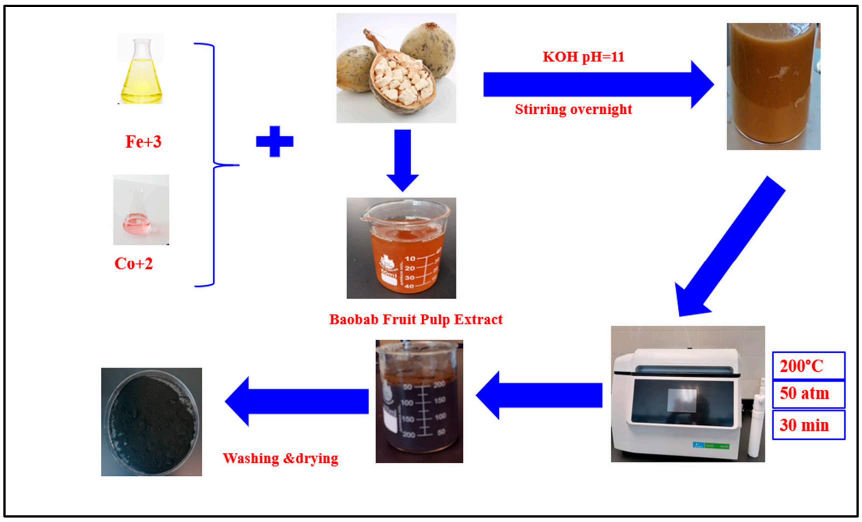

Figure 12. Schematic diagram of the synthesis of $CoFe_2O_4$ nanocomposite.

3.4. Assessment of the Antibacterial Inhibitory Potentials of $CoFe_2O_4$ Nanoparticles

To examine the antimicrobial behavior of the synthesized $CoFe_2O_4$ nanoparticles, the OD method was applied at 600 nm. An antibacterial assessment of $CoFe_2O_4$ NPs was performed against five species of human pathogenic bacteria: *Escherichia coli*, Marsa, Pseudomonas aeruginosa, Klebsiella Pseudomonas, and Candida, as well as one fungal species. $CoFe_2O_4$ nanoparticles were prepared in different concentrations (0, 2, 4, 8, 12, and 16) to examine their antimicrobial activity against pathogenic microorganisms. A total of 20 ppm of amoxicillin antibiotic was used for comparison. Nutrient broth (NB) medium was prepared and used as a suspension for the prepared $CoFe_2O_4$ nanoparticles. An inoculum from the pathogenic culture (100 µL) in the logarithmic phase was injected into the nutrient broth medium, which had previously been amended with the nanoparticles (5 mL) under aseptic conditions. All samples were incubated for 24 h at 30 °C, and their absorbance was recorded spectrophotometrically at 600 nm.

3.5. Characterization

The morphological structure of the synthesized $CoFe_2O_4$ nanoparticles was studied using a field-emission scanning electron microscope (FE-SEM model FEI, QUANTA FEG, 250) from Hillsboro, OR, USA, fitted with a high-angle, angular dark-field detector and X-ray energy dispersive spectroscopy system (EDX). The structural phase was detected using X-ray diffraction (XRD) with a Shimadzu XRD-7000 with an X-ray wavelength Cu detector, sourced from Kyoto, Japan. The structural analysis was performed using Fourier-transform infrared spectroscopy (FTIR) (Shimadzu IR Tracer-100 FTIR Spectrophotometer, NC, USA) in the wavelength range of 4000 to 400 cm^{-1}. Specific surface area, total pore volume and pore size distribution were measured using a Brunauer–Emmett–Teller (BET) surface-area analyzer, Osaka, Japan.

3.6. Catalytic Dye Degradation Experiment

The adsorption of MO using $CoFe_2O_4$ nanoparticles was conducted in batch experiments under numerous parameters to show their effect on the adsorption of MO dye. These parameters included the pH of the dye, the dye concentration, the contact time, and finally the adsorbent dosage. A batch experiment was conducted using 20 mL of MO solution with concentrations varying from 10 to 50 mg/L at pH 3 at room temperature. The pH of the solution was adjusted using 1 M HCL and 1 M NaOH and varied from 2 to 11. Various adsorbent doses (0.01 to 0.1 g) were added to the MO solution with an initial concentration of 20 mg/L to study the effect of adsorbent dosages on MO adsorption. The mixture was shaken at room temperature, 350 rpm, and left for 24 h to ensure that it reached equilibrium. The MO concentration (C_t) was measured at a wavelength of 463 nm using a UV–vis spectrophotometer. All experiments were performed two times, and the average of the values was used in the study. The amount of dye removal at equilibrium at different time intervals in the range 0–120 min was calculated using Equation (5),

$$removal\ percentage\ of\ MO = \frac{(C_o - C_t)}{C_o} \times 100 \tag{5}$$

where C_o and C_t (mg/L) are the initial concentration and concentration at time t, respectively, of the MO solution and the MO.

4. Conclusions

An eco-friendly, sustainable, cost-effective, and simple approach was applied in this study for the synthesis of $CoFe_2O_4$ nanoparticles by using *Adansonia digitata* L. (Baobab) Fruit Pulp Extract assisted by the microwave heating method. This method generates nanoscale materials that are free from hazardous or harmful chemicals and that are considered environmentally friendly, sustainable materials. To the best of our knowledge, there is no previous study on using *Adansonia digitata* L. (Baobab) Fruit Pulp Extract for the synthesis of $CoFe_2O_4$ nanoparticles as a capping and reducing agent. Different techniques were used to confirm the successful synthesis of $CoFe_2O_4$ nanoparticles. FT-IR results confirmed that polyphenols and flavonoids present in *Adansonia digitata* L. (Baobab) Fruit Pulp Extract are critical for the synthesis of nanoparticles. SEM and TEM analysis confirmed the spherical and regular shape of nanoparticles with an average size of around 31.5 nm. Magnetic analysis of cobalt ferrite nanoparticles displayed ferromagnetic properties with a saturation magnetization (Ms) value equal to 56 emu/g. The $CoFe_2O_4$ nanoparticles displayed excellent dye removal efficiency (97.5%) achieved at pH 2.8. The kinetics experiments described a pseudo-second-order kinetic model as the best fit model with (0.9844) R^2 values comparable to pseudo-first-order (R^2 = 0.8084). The isotherm study displayed that the Freundlich isotherm model is the best fit to the experimental data, which supports the monolayer loading of MO dye molecules onto the surface of $CoFe_2O_4$ nanoparticles. In addition, significant antimicrobial activity was achieved by $CoFe_2O_4$ nanoparticles towards different bacterial Gram classes. Both their catalytic and antimicrobial activity make the sustainably synthesized $CoFe_2O_4$ nanoparticles a promising candidate for environmental and medical applications.

Author Contributions: Conceptualization, A.T. and N.A.; methodology, A.T.; software, A.T.; validation, A.T. and N.A.; formal analysis, A.T.; investigation, N.A.; resources, A.T.; data curation, A.T.; writing—original draft preparation, A.T. and N.A.; writing—review and editing, A.T.; visualization, A.T. and N.A. supervision, A.T.; project administration, A.T. and N.A.; funding acquisition, N.A. All authors have read and agreed to the published version of the manuscript.

Funding: This work was supported by the Deanship of Scientific Research, Vice Presidency for Graduate Studies and Scientific Research, King Faisal University, Saudi Arabia [Grant No. KFU262275].

Institutional Review Board Statement: Not applicable.

Informed Consent Statement: Not applicable.

Data Availability Statement: The original contributions presented in this study are included in the article. Further inquiries can be directed to the corresponding author.

Acknowledgments: The authors extend their appreciation to the Deanship of Scientific Research, Vice Presidency for Graduate Studies and Scientific Research, King Faisal University, Saudi Arabia [Grant No. KFU262275].

Conflicts of Interest: The authors declare no conflicts of interest.

References

1. Daffalla, S.; Da'na, E.; Taha, A.; El-Aassar, M.R. Synthesis of a Novel Magnetic Biochar from Lemon Peels via Impregnation-Pyrolysis for the Removal of Methyl Orange from Wastewater. *Magnetochemistry* **2024**, *10*, 95. [CrossRef]
2. Dutta, B.; Gupta, S.; Srivastava, K.; Gupta, A.K. Recent advances on the removal of dyes from wastewater using various adsorbents: A critical review. *Mater. Adv.* **2021**, *2*, 4497–4531. [CrossRef]
3. Wang, S.-S.; Yan, Y.-M.; Hsu, C.-H.; Lin, H.-P. Waste bamboo-derived biochar and multiporous carbon as adsorbents for methyl orange removal. *J. Chin. Chem. Soc.* **2023**, *70*, 1628–1635. [CrossRef]
4. Haziq, A.; Gholipour, A.; Farha, S. Adsorptive removal of toxic organic dyes from water by using a magnetic dual metal-organic framework hybrid (MIL-53(Fe)@MIL-101(Fe)/$CoFe_2O_4$) as a novel fast nano-adsorbent. *Inorg. Chem. Res.* **2024**, *8*, 32–45. [CrossRef]
5. Wei, F.; Zhang, H.; Ren, Q.; Chen, H.; Yang, L.; Ding, B.; Yu, M.; Liang, Z. Removal of organic contaminants from wastewater with GO/MOFs composites. *PLoS ONE* **2021**, *16*, e0253500. [CrossRef] [PubMed]
6. Priyanka, K.; Suresh, H.K.; Mathad, S.N.; Shedam, R.; Shedam, M.R. A Review on Synthesis, Properties and Applications on Cobalt Ferrite. *Int. J. Adv. Sci. Eng.* **2022**, *9*, 2567–2583. [CrossRef]
7. Lee, S.; Bae, S.; Takemura, S.; Shim, Y.; Kim, I.-B.; Kim, T.; Lee, J.; Zurn, H.; Kim, S. Self-heating characteristics of cobalt ferrite nanoparticles for hyperthermia application. *J. Magn. Magn. Mater.* **2007**, *310*, 2868–2870. [CrossRef]
8. Salih, S.J.; Mahmood, W.M. Review on magnetic spinel ferrite (MFe_2O_4) nanoparticles: From synthesis to application. *Heliyon* **2023**, *9*, e16601. [CrossRef] [PubMed]
9. Dippong, T.; Levei, E.A.; Cadar, O. Recent advances in synthesis and applications of MFe_2O_4 (M = Co, Cu, Mn, Ni, Zn) nanoparticles. *Nanomaterials* **2021**, *11*, 1560. [CrossRef] [PubMed]
10. Abdulhamid, Z.; Dabbawala, Z.; Delclos, A.; Straubinger, T.; Rueping, R.; Polychronopoulou, M.; Anjum, K. Synthesis, characterization, and preliminary insights of $ZnFe_2O_4$ nanoparticles into potential applications, with a focus on gas sensing. *Sci. Rep.* **2023**, *13*, 19750. [CrossRef] [PubMed]
11. Datt, G.; Kotabage, C.; Abhyankar, A.C. Ferromagnetic resonance of $NiCoFe_2O_4$) nanoparticles and microwave absorption properties of flexible NiCoFe2O4-carbon black/poly(vinyl alcohol) composites. *Phys. Chem.* **2017**, *19*, 20699–20712. [CrossRef] [PubMed]
12. Al Kiey, S.A.; Ahmad, M.M.; Azab, A.A. Tailoring cobalt-doped nickel ferrite nanostructures for high-performance supercapacitors. *J. Energy Storage* **2026**, *148*, 119968. [CrossRef]
13. Omar, B.A.; Hasan, M.A.; Abed, N.S. Characterization and Application of $ZnFe_2O_4$ Soft Ferrite: A Review. *Eur. J. Appl. Sci. Eng. Technol.* **2026**, *4*, 10. [CrossRef]
14. Hernandez-fuerte, L.D.; De Jesús, T. Optimization of adsorption of methyl orange from aqueous solution by magnetic $CoFe_2O_4$/ZnAl-layered double hydroxide composite using response surface methodology. *Mater. Res. Express* **2023**, *10*, 015505. [CrossRef]
15. Sulaiman, J.M.A.; Hamdoon, S.M.; Abdulrahman, G.Y. Antibacterial Activity of Cobalt Ferrite ($CoFe_2O_4$) Nanoparticles against Oral Enterococci. *Mater. Sci. Forum* **2021**, *1021*, 150–159. [CrossRef]
16. Peymanfar, R.; Azadi, F.; Yassi, Y. Preparation and Characterization of $CuFe_2O_4$ Nanoparticles by the Sol-Gel Method and Investigation of Its Microwave Absorption Properties at Ku-Band Frequency Using Silicone Rubber. *Proceedings* **2018**, *2*, 1155. [CrossRef]
17. Simonescu, C.M.; Tătăruş, A.; Culiţă, D.C.; Stănică, N.; Ionescu, I.A.; Butoi, B.; Banici, A.-M. Comparative Study of $CoFe_2O_4$ Nanoparticles and $CoFe_2O_4$-Chitosan Composite for Congo Red and Methyl Orange Removal by Adsorption. *Nanomaterials* **2021**, *11*, 711. [CrossRef] [PubMed]
18. Taha, A. Microwave-Sample-Preparation-System-Assisted Biogenic Synthesis of Copper Oxide Nanoplates Using Saussurea costus Root Aqueous Extract and Its Environmental Catalytic Activity. *Catalysts* **2022**, *12*, 1115. [CrossRef]
19. Taha, A.; Alsadun, N. High efficiency reduction of 4-nitrophenol on greenly synthesized gold nanoparticles decorated on chitosan matrix (CS-GLA/AuNPs). *Sci. Rep.* **2025**, *15*, 36333. [CrossRef] [PubMed]
20. Al-Radadi, N.S. Saussurea costus for sustainable and eco-friendly synthesis of palladium nanoparticles and their biological activities. *Arab. J. Chem.* **2022**, *15*, 104294. [CrossRef]
21. Thompson, P.T.; Boamah, V.E.; Badu, M. In-vitro antioxidant, antimicrobial and phytochemical properties of extracts from the pulp and seeds of the African baobab fruit (*Adansonia digitata* L.). *Heliyon* **2024**, *10*, e29660. [CrossRef] [PubMed]

22. Zeebaree, A.Y.S.; Abdel Rasool, A.M.; ALkhyatt, M.M. View of baobab extract with zinc oxide nanoparticles for targeted treatment for liver cancer. *Int. J. App Pharm.* **2026**, *18*, 306–313. [CrossRef]
23. Kumar, C.M.; Yugandhar, P.; Savithramma, N. Biological synthesis of silver nanoparticles from *Adansonia digitata* L. fruit pulp extract, characterization, and its antimicrobial properties. *J. Intercult. Ethnopharmacol.* **2016**, *5*, 79. [CrossRef] [PubMed]
24. Tamboli, Y.; Patange, S.M.; Mohanta, Y.K.; Sharma, R.; Zakde, K.R. Green Synthesis of Cobalt Ferrite Nanoparticles: An Emerging Material for Environmental and Biomedical Applications. *J. Nanomater.* **2023**, *15*, 9770212. [CrossRef]
25. Kombaiah, K.; Vijaya, J.J.; Kennedy, L.J.; Bououdina, M.; Ramalingam, R.J.; Al-Lohedan, H.A. Okra extract-assisted green synthesis of $CoFe_2O_4$ nanoparticles and their optical, magnetic, and antimicrobial properties. *Mater. Chem. Phys.* **2017**, *204*, 410–419. [CrossRef]
26. Velayutham, L.; Parvathiraja, C.; Anitha, D.C.; Mahalakshmi, K.; Jenila, M.; Alasmary, F.A.; Almalki, A.S.; Iqbal, A.; Lai, W.-C. Photocatalytic and Antibacterial Activity of CoFe2O4 Nanoparticles from Hibiscus rosa-sinensis Plant Extract. *Nanomaterials* **2022**, *12*, 3668. [CrossRef] [PubMed]
27. Dichayal, S.; Murade, V.; Deshmukh, S.; Pansambal, S.; Hase, D.; Oza, R. Green Synthesis of Cobalt Ferrite Nanoparticles: A Comprehensive Review on Eco-friendly Approaches, Characterization Techniques, and Potential Applications. *J. Chem. Rev.* **2024**, *6*, 514–531. [CrossRef]
28. Abdelsattar, A.S.; Kamel, A.G.; El-Shibiny, A. The green production of eco-friendly silver with cobalt ferrite nanocomposite using Citrus limon extract. *Results Chem.* **2023**, *5*, 100687. [CrossRef]
29. Mdlalose, W.B.; Mokhosi, S.R.; Dlamini, S.; Moyo, T.; Singh, M. Effect of chitosan coating on the structural and magnetic properties of $MnFe_2O_4$ and $Mn_{0.5}Co_{0.5}Fe_2O_4$ nanoparticles. *AIP Adv.* **2018**, *8*, 056726. [CrossRef]
30. Vunain, E.; Kenneth, D.; Biswick, T. Synthesis and characterization of low-cost activated carbon prepared from Malawian baobab fruit shells by H_3PO_4 activation for removal of Cu(II) ions: Equilibrium and kinetics studies. *Appl. Water Sci.* **2017**, *7*, 4301–4319. [CrossRef]
31. Song, S.; Abubaker, M.A.; Akhtar, M.; Elimam, A.M.; Zhu, X.; Zhang, J. Chemical Characterization Analysis, Antioxidants, and Anti-Diabetic Activity of Two Novel Acidic Water-Soluble Polysaccharides Isolated from Baobab Fruits. *Foods* **2024**, *13*, 912. [CrossRef] [PubMed]
32. Wu, X.; Wang, W.; Li, F.; Khaimanov, S.; Tsidaeva, N.; Lahoubi, M. PEG-assisted hydrothermal synthesis of $CoFe_2O_4$ nanoparticles with enhanced selective adsorption properties for different dyes. *Appl. Surf. Sci.* **2016**, *389*, 1003–1011. [CrossRef]
33. Charbgoo, F.; Bin Ahmad, M.; Darroudi, M. Cerium oxide nanoparticles: Green synthesis and biological applications. *Int. J. Nanomed.* **2017**, *12*, 1401–1413. [CrossRef] [PubMed]
34. Mallesh, S.; Srinivas, V. Evolution of structure and magnetic properties in MnZn ferrite-silica nanocomposites fabricated by sol–gel method. *J. Mater. Sci. Mater. Electron* **2021**, *32*, 4862–4871. [CrossRef]
35. Šuljagić, M.; Vulić, P.; Jeremić, D.; Pavlović, V.; Filipović, S.; Kilanski, L.; Lewinska, S.; Slawska-Waniewska, A.; Milenković, M.R.; Nikolić, A.S.; et al. The influence of the starch coating on the magnetic properties of nanosized cobalt ferrites obtained by different synthetic methods. *Mater. Res. Bull.* **2021**, *134*, 111117. [CrossRef]
36. Ibiyemi, A.A.; Akinrinola, O.; Yusuf, G.T. Photoelectric and optoelectronic effects of hard ferromagnetic man-ganese cobalt (Mn–Co) ferrite nanoparticles for high-frequency device application. *Appl. Phys. A* **2022**, *128*, 792. [CrossRef]
37. Abdullah, M.; Hasany, S.; Amir Qureshi, M.; Hussain, S. Cost-Effective Synthesis of Cobalt Ferrite Nanoparticles by Sol-Gel Technique. *MSF* **2022**, *1067*, 213–219. [CrossRef]
38. Caldeira, L.E.; Erhardt, C.S.; Mariosi, F.R.; Venturini, J.; Zampiva, R.Y.S.; Montedo, O.R.K.; Arcaro, S.; Bergmann, C.P.; Bragança, S.R. Correlation of synthesis parameters to the structural and magnetic properties of spinel cobalt ferrites ($CoFe_2O_4$)—An experimental and statistical study. *J. Magn. Magn. Mater.* **2022**, *550*, 169128. [CrossRef]
39. Bhowmik, M.; Kanmani, M.; Debnath, A.; Saha, B. Sono-assisted rapid adsorption of anionic dye onto magnetic $CaFe_2O_4/MnFe_2O_4$ nanocomposite from aqua matrix. *Powder Technol.* **2019**, *354*, 496–504. [CrossRef]
40. Kapur, M.D.; Janani, M.; Jeyaraman, R.; Natarajan, P.; Djearamane, A.; Shing, S.L.; Kayarohanam, W. Simple biotic; spinel $CoFe_2O_4$ nanosphere for textile pollutant removal by photoresponsivity process and Anti-Microbial analysis. *J. King Saud. Univ. Sci.* **2024**, *36*, 103369. [CrossRef]
41. Kubendiran, H.; Hui, D.; Pulimi, M.; Chandrasekaran, N.; Murthy, P.S.; Mukherjee, A. Removal of methyl orange from aqueous solution using SRB supported Bio-Pd/Fe NPs. *Environ. Nanotechnol. Monit. Manag.* **2021**, *16*, 100561. [CrossRef]
42. Arshadi, M.; Salimivahid, F.; Salvacion, J.W.L.; Soleymanzadeh, M. Adsorption studies of methyl orange on an immobilized Mn-nanoparticle: Kinetic and thermodynamic. *RSC Adv.* **2014**, *8*, 16005–16017. [CrossRef]
43. Revathi, J.; Abel, M.J.; Archana, V.; Sumithra, T.; Thiruneelakandan, R.; Joseph Prince, J. Synthesis and characterization of $CoFe_2O_4$ and Ni-doped $CoFe_2O_4$ nanoparticles by chemical Co-precipitation technique for photo-degradation of organic dyestuffs under direct sunlight. *Phys. B Condens. Matter* **2020**, *587*, 412136. [CrossRef]
44. Sirajudheen, P.; Karthikeyan, P.; Basheer, M.C.; Meenakshi, S. Adsorptive removal of anionic azo dyes from effluent water using Zr(IV) encapsulated carboxymethyl cellulose-montmorillonite composite. *Environ. Chem. Ecotoxicol.* **2020**, *2*, 73–82. [CrossRef]

45. Da'na, E.; Hassanin, H.A.; Taha, A.; El-Aassar, M.R. Microwave-Aided Green Synthesis of ZrO_2/ZnO/AC Nanocomposite for Catalytic Degradation of Organic Dye. *Water Air Soil Pollut.* **2023**, *234*, 436. [CrossRef]
46. Zhu, H.Y.; Jiang, R.; Xiao, L.; Zeng, G.M. Preparation, characterization, adsorption kinetics and thermodynamics of novel magnetic chitosan enwrapping nanosized γ-Fe_2O_3 and multi-walled carbon nanotubes with enhanced adsorption properties for methyl orange. *Bioresour. Technol.* **2010**, *101*, 5063–5069. [CrossRef] [PubMed]
47. Rekaby, M. Preparation and characterization of a novel nanocomposite based on MnCr-layered double oxide and $CoFe_2O_4$ spinel ferrite for methyl orange adsorption. *Sci. Rep.* **2023**, *13*, 18006. [CrossRef] [PubMed]
48. El-Sayed, E.-S.R.; Abdelhakim, H.K.; Zakaria, Z. Extracellular biosynthesis of cobalt ferrite nanoparticles by *Monascus purpureus* and their antioxidant, anticancer and antimicrobial activities: Yield enhancement by gamma irradiation. *Mater. Sci. Eng. C* **2020**, *107*, 110318. [CrossRef] [PubMed]
49. Mahajan, P.; Sharma, A.; Kaur, B.; Goyal, N.; Gautam, S. Green synthesized (*Ocimum sanctum* and *Allium sativum*) Ag-doped cobalt ferrite nanoparticles for antibacterial application. *Vacuum* **2019**, *161*, 389–397. [CrossRef]
50. Satheeshkumar, P.; Ranjith Kumar, M.K.; Srinivas, E.; Suriyanarayanan, C.; Deepty, N.; Prajapat, M.; Lal Rao, C.; Sastry, T.; Devulapalli. Study of structural, morphological and magnetic properties of Ag substituted cobalt ferrite nanoparticles prepared by honey assisted combustion method and evaluation of their antibacterial activity. *J. Magn. Magn. Mater.* **2019**, *469*, 691–697. [CrossRef]
51. Naik, M.M.; Naik, H.S.B.; Nagaraju, G.; Vinuth, M.; Vinu, K.; Viswanath, R. Green synthesis of zinc doped cobalt ferrite nanoparticles: Structural, optical, photocatalytic and antibacterial studies. *Nano-Struct. Nano-Objects* **2019**, *19*, 100322. [CrossRef]